Spontaneous emission interference in negative-refractive-index waveguides

Gao-xiang Li,[1,2,*] Jörg Evers,[1,†] and Christoph H. Keitel[1]
[1]*Max-Planck-Institut für Kernphysik, Saupfercheckweg 1, D-69117 Heidelberg, Germany*
[2]*Department of Physics, Huazhong Normal University, Wuhan 430079, China*
(Received 17 February 2009; revised manuscript received 29 April 2009; published 2 July 2009)

The spontaneous decay of a *V*-type three-level atom placed in a negative-refractive-index waveguide is analyzed. We find that in thin waveguides, highly efficient surface-guided modes are supported, which do not occur in positive-index waveguides. In addition, at low absorption, the mode density and thus spontaneous emission into particular regular-guided modes is enhanced by several orders of magnitude as compared to regular dielectric waveguides. The asymmetries between emission into the different modes and the enhancement of particular guided modes allow us to induce strong spontaneous emission interference between transitions with orthogonal transition dipole moments.

DOI: 10.1103/PhysRevB.80.045102 PACS number(s): 78.20.Bh, 78.20.Ci, 42.50.Gy, 42.50.Pq

I. INTRODUCTION

Spontaneous emission (SE) of atoms is not an immutable property but can be altered essentially via two different mechanisms. One mechanism involves modification of the internal dynamics. For example, quantum interference among different decay channels of the atom can be established, such that spontaneous emission is modified to a great extend.[1,2] A particular class of quantum interference schemes that has received much theoretical attention in the literature is based on so-called spontaneously generated coherences (SGC). These coherences have, for example, been shown to lead to quenching of spontaneous emission,[3] narrow spectral lines,[4] phase-dependent line shapes,[5] rapid phase control of collective population dynamics,[6] and lasing without inversion.[7] Despite the large theoretical interest, there is no experimental proof of this type of SGC in atomic systems due to the lack of appropriate candidate systems. The reason for this is that SGC-based interference requires the presence of near-degenerate atomic transitions with near-(anti)parallel dipole moments sharing a common atomic state, which does not occur in real atoms.[1] To circumvent this in atoms, schemes to simulate interference or to induce interference by external driving fields have been considered[1,8] but so far without clear experimental implementation. An experimental observation of SGC in molecules[9] could not be confirmed in a repetition of the experiment.[10] SGC have been observed, however, in artificial quantum systems, where a suitable level scheme can be designed.[11] Also, it has been recognized that a more general form of SGC occurs between near-degenerate atomic transitions with near-(anti)parallel dipole moments that do not share a common state. This generalized SGC may lead to measurable effects in realistic atomic systems.[12] These generalized SGC are also a common interpretation for the occurrence of electromagnetically induced absorption.[13]

The second major mechanism for a modification of spontaneous emission is to modify the electromagnetic boundary conditions surrounding the atom, such as in cavities.[14] Recently, it has been shown that a favorable modification of the boundary conditions is possible in media having a negative-refractive index (NRI). NRI currently receive a lot of attention because of both experimental demonstrations and potential applications.[15] For example, NRI material allows to realize superlenses which, in principle, can achieve arbitrary subwavelength resolution.[16] Experimentally, the NRI materials have been realized over a wide range of frequencies, from the microwave up to the optical range.[17,18] It has been shown[19] that a single layer of a NRI material has broadband omnidirectional reflection properties. In the range between the electric plasma frequency and the magnetic plasma frequency, the refractive index is close to zero and the NRI materials reflect radiation for angles of incidence and polarization with reflectivity of ~ 0.99. By exploiting the reflective phase properties of the NRI materials, an all-dimensional subwavelength resonator[20] has been designed and fabricated. In the field of quantum optics, two atoms placed at the foci of a perfect lens formed by a NRI slab exhibit perfect subradiance and super-radiance over macroscopic distances.[21] Such focusing and phase compensation can also be used to induce quantum interference.[22] In a NRI slab waveguide,[23–25] surface-guided modes may exist for imaginary transverse wave numbers with power concentrated at the interfaces rather than inside the slab. In an air waveguide with NRI cladding,[26] both transverse electric and magnetic modes can be supported with low losses. The existence of the transverse electric (TE) surface-guided modes in the NRI slab waveguide, where the permeability changes its sign at the interface, resemble the transverse magnetic (TM) surface-plasmon-polariton modes at the interface between the metal and the dielectric, where the permittivity changes its sign.[27] Plasmonic-based nanophotonic devices have attracted much interest from the quantum optics community for their use in quantum information processing.[28] A technique which enables strong coherent coupling between individual optical emitters and guided plasmon excitations in conducting nanostructure at optical frequencies has been proposed.[29] In view of these remarkable properties of NRI structures, the question arises, how spontaneous emission is modified in such a surrounding.

Therefore, here we study the SE of an atom embedded in the middle layer of NRI slab waveguides. The atom is modeled as a *V*-type three-level atom with orthogonal dipole moments on the dipole-allowed transitions as it is the case in real atoms. The NRI layer is described using a Drude-

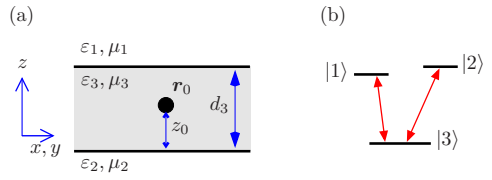

FIG. 1. (Color online) Schematic setup for spontaneous decay in a waveguide with negative index of refraction material. (a) The waveguide consists of an inner layer with material parameters ϵ_3, μ_3, and thickness d_3. It is surrounded by infinite outer layers with material parameters ϵ_i and $\mu_i (i \in \{1,2\})$. In the middle layer, an atom is embedded at position $\mathbf{r}_0$. (b) Electronic structure of the embedded atom, which is a three-level atom in V-type configuration.

Lorentz model including dispersion and absorption. The different contributions to SE are first classified and interpreted using approximate analytical results. Then, we verify our results via numerical calculations. We find that at low absorption, the SE rate into particular waveguide modes can be several orders of magnitude larger than the free space rate due to a strong enhancement of the mode density. Further, in thin waveguides, a dominant contribution to SE arises from surface-guided modes, which do not occur in regular positive-index waveguides. At high absorption, the strong enhancement of waveguide modes is reduced while the surface-guided mode contribution remains several orders of magnitude higher than free space decay. As our main result, we show that the asymmetric mode structure and the strong enhancement of particular modes can be used to engineer spontaneous emission interference between the two transitions in the embedded atom. Thus we find that the NRI waveguide allows to induce and control near-perfect quantum interference in realistic atomic-level schemes.

II. MODEL

We consider a V-type three-level atom embedded in the middle layer of a three-layer waveguide as shown in Fig. 1. The upper levels could be Zeeman sublevels $|1\rangle = |j=1, m=1\rangle$ and $|2\rangle = |j=1, m=-1\rangle$ with energies $\hbar\omega_1$ and $\hbar\omega_2$, and we set the ground-state $|3\rangle = |j=0, m=0\rangle$ energy to zero in the following. The y direction is the quantization axis (e.g., by applying a weak static magnetic), and the direction normal to the layer interfaces the z axis. Then, the atomic dipole moment operator is given by

$$\mathbf{d} = d(A_{13}\mathbf{e}_1 + A_{23}\mathbf{e}_2) + \text{H.c.}, \tag{1}$$

where

$$\mathbf{e}_{1,2} = \frac{1}{\sqrt{2}}(\mathbf{e}_z \pm i\mathbf{e}_x), \tag{2}$$

and $A_{ij} = |i\rangle\langle j| (i,j \in \{1,2,3\})$ are the atomic transition $(i \neq j)$ and population $(i=j)$ operators. $\mathbf{e}_k (k \in \{x,y,z\})$ are the normalized Cartesian basis vectors and d is the atomic-dipole strength, chosen to be real. We denote the dielectric permittivity and the magnetic permeability of the layer cladding the atom as $\varepsilon_3(\omega)$ and $\mu_3(\omega)$, which we obtain from a Drude-Lorentz model

$$\varepsilon_3(\omega) = 1 + \frac{\omega_{pe}^2 - \omega_{Te}^2}{\omega_{Te}^2 - \omega^2 - i\omega\gamma_e}, \tag{3a}$$

$$\mu_3(\omega) = 1 + \frac{\omega_{pm}^2 - \omega_{Tm}^2}{\omega_{Tm}^2 - \omega^2 - i\omega\gamma_m}. \tag{3b}$$

Here, $\omega_{pe}(\omega_{pm})$, $\omega_{Te}(\omega_{Tm})$, and $\gamma_e(\gamma_m)$ are electric (magnetic) coupling constant, medium oscillation frequency, and linewidth, respectively. The permittivity and permeability of the upper (lower) layer, which extends to infinity in the positive (negative) z direction, are $\varepsilon_2(\omega)$ and $\mu_2(\omega)$ [$\varepsilon_1(\omega)$ and $\mu_1(\omega)$]. For these, we assume low absorption and choose ε_j, μ_j $(j \in \{1,2\})$ as real.[21,23,30] d_3 is the thickness of the middle layer. In the interaction picture, the master equation for the density matrix ρ is[8]

$$\frac{d}{dt}\rho = \sum_{n=1}^{2} \Gamma_n(\rho_{nn}A_{33} - A_{nn}\rho) + \sqrt{\Gamma_1\Gamma_2} \times \sum_{n\neq m=1}^{2} \kappa_n(A_{mn}\rho - \rho_{nm}A_{33}) + \text{H.c.} \tag{4}$$

Here, Γ_n are spontaneous emission rates[31]

$$\Gamma_n = \frac{d^2\omega_n^2}{\hbar\varepsilon_0 c^2}\mathbf{e}_\mathbf{n}^* \cdot \mathbf{G}_{\text{Im}} \cdot \mathbf{e}_\mathbf{n} = \Gamma_{nx} + \Gamma_{nz}, \tag{5}$$

with polarization components Γ_{nx} and Γ_{nz}. The terms involving κ_1 and κ_2 in Eq. (4) are responsible for quantum interference between the two SE channels $|1\rangle \rightarrow |3\rangle$ and $|2\rangle \rightarrow |3\rangle$ with κ_n given by

$$\kappa_n = \frac{d^2\omega_1\omega_2}{\hbar\varepsilon_0 c^2\sqrt{\Gamma_1\Gamma_2}}\mathbf{e}_\mathbf{n} \cdot \mathbf{G}_{\text{Im}} \cdot \mathbf{e}_\mathbf{n} = \frac{\Gamma_{nz} - \Gamma_{nx}}{\sqrt{\Gamma_1\Gamma_2}}. \tag{6}$$

Here, $-1 \leq \kappa_1, \kappa_2 \leq 1$ describes the degree of interference, and $\mathbf{r}_0 = (x_0, y_0, z_0)^T$ is the position of the atom in the middle layer. $\mathbf{G}_{\text{Im}} = \text{Im}[\mathbf{G}(\mathbf{r}_0, \mathbf{r}_0, \omega_n)]$ is the imaginary part of the electromagnetic Green tensor $\mathbf{G}(\mathbf{r}_0, \mathbf{r}_0, \omega)$ given by[32]

$$\mathbf{G}(\mathbf{r}_0, \mathbf{r}_0, \omega) = \frac{i\mu_3}{8\pi\tilde{k}_3^2}\int_0^\infty \frac{dkk}{\beta_3}\left[(\mathbf{e}_z\mathbf{e}_z)\frac{2k^2}{D_{p3}}\mathcal{I}_+^{(p)} + (\mathbf{e}_x\mathbf{e}_x + \mathbf{e}_y\mathbf{e}_y) \times \left(\frac{\beta_3^2}{D_{p3}}\mathcal{I}_-^{(p)} + \frac{\tilde{k}_3^2}{D_{s3}}\mathcal{I}_+^{(s)}\right)\right]. \tag{7}$$

Here,

$$\mathcal{I}_\pm^{(q)} = (1 \pm r_{31}^q e^{2i\beta_3 z_0})(1 \pm r_{32}^q e^{2i\beta_3(d_3 - z_0)}), \tag{8a}$$

$$\tilde{k}_j^2 = \eta_j\omega^2/c^2, \tag{8b}$$

$$\eta_j = \varepsilon_j(\omega)\mu_j(\omega), \tag{8c}$$

with $j \in \{1,2,3\}$. The parameter k is the magnitude of the vector $\mathbf{k} = (k_x, k_y)^T$, the conserved component of the wave vector, which is parallel to the interfaces of the layers. The β_j $(j \in \{1,2,3\})$ are the magnitude of the z component of the wave vector in the jth layer, whose definition depends on the refraction index of the jth layer and the value of k.[33] If

$\mathrm{Re}(k)<\mathrm{Re}(\tilde{k}_j)$, that is, the corresponding wave in the jth layer is a propagating one, then β_j is expressed as $\beta_j=(\tilde{k}_j^2-k^2)^{1/2}$ if the jth layer has positive refraction index, and $\beta_j=-(\tilde{k}_j^2-k^2)^{1/2}$ when the jth if the layer is a left-handed material. Here, $\mathrm{Re}(x)$ is the real part of x.

On the other hand, if $\mathrm{Re}(k)>\mathrm{Re}(\tilde{k}_j)$ corresponding to an evanescent wave in the jth layer then $\beta_j=i(k^2-\tilde{k}_j^2)^{1/2}$ independent of the type of the jth layer. Following Ref. 32, we denote the electric field of the TM [TE] wave by the index p [s]. The functions $D_{q3}(q\in\{p,s\})$ are defined as

$$D_{q3}=1-r_{31}^q r_{32}^q e^{2i\beta_3 d_3}, \tag{9}$$

where r_{31}^q and r_{32}^q are reflection coefficients given by

$$r_{ij}^p=\frac{\varepsilon_j\beta_i-\varepsilon_i\beta_j}{\varepsilon_j\beta_i+\varepsilon_i\beta_j}, \quad r_{ij}^s=\frac{\mu_j\beta_i-\mu_i\beta_j}{\mu_j\beta_i+\mu_i\beta_j}. \tag{10}$$

From Eq. (7) we can see that the inhomogeneity of the medium along the z axis leads to a spatially asymmetric Green's tensor as the z component is different from those in the x-y plane. For notational simplicity, in the following β_3 and k will be rescaled by ω/c, i.e., $\beta_3/(\omega/c)$ and $k/(\omega/c)$ will be replaced by β_3 and k. As usual, the permittivity and permeability coefficients of the three layers are assumed to obey $\mathrm{Re}(\eta_3)>\mathrm{Re}(\eta_1)\geq\mathrm{Re}(\eta_2)$. Then the electromagnetic modes in this structure can be classified into radiation modes with $0<\mathrm{Re}(k^2)<\mathrm{Re}(\eta_2)$, substrate modes with $\mathrm{Re}(\eta_2)<\mathrm{Re}(k^2)<\mathrm{Re}(\eta_1)$, regular-guided modes with $\mathrm{Re}(\eta_1)<\mathrm{Re}(k^2)<\mathrm{Re}(\eta_3)$, and evanescent modes with $\mathrm{Re}(k^2)>\mathrm{Re}(\eta_3)$. As quantum interference requires near-degenerate transition frequencies, we also assume $\omega_1\approx\omega_2=\omega$ so that $\Gamma_1\approx\Gamma_2=\Gamma$ and $\kappa_1\approx\kappa_2=\kappa$.

III. RESULTS

We assume that both the upper and the lower layers are dielectric media with positive refraction index and the middle layer surrounding the atom is left-handed material. This structure is a so-called NRI waveguide.[23] The contributions of the radiation and the substrate modes to the SE rate can be obtained by integrating Eq. (7) numerically. An example is shown in Fig. 2(a). For the following analytical considerations, we assume ε_3 and μ_3 to be constant and real, i.e., we neglect absorption and dispersion. But our numerical results include both absorption and dispersion.

A. Waveguide modes

The regular-guided modes have complex reflection coefficients with modulus 1. In this region, the imaginary parts of the integrands in Eq. (7) are zero, apart from resonances when $D_{q3}=0$ $(q\in\{p,s\})$ is satisfied. For example, the SE rate of the z component of the atomic dipole moment into p-polarized guided modes is

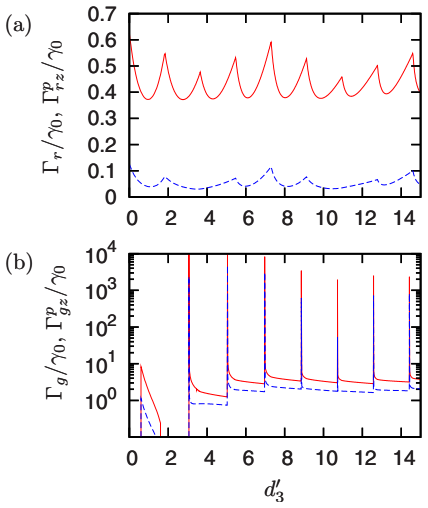

FIG. 2. (Color online) (a) Radiation modes with total rate Γ_r (red solid line) and contribution Γ_{rz}^p of the p mode for z polarization (blue dashed). (b) Waveguide modes with total rate Γ_g (red solid line) and contribution Γ_{gz}^p of the p mode for z polarization (blue dashed). The atom is located at $z_0'=0.25d_3'$, and the material parameters are $\varepsilon_1=\varepsilon_2=\mu_1=\mu_2=1.0$, $\omega_{pe}=\omega_{pm}=1.32\omega_0$, $\omega_{Te}=\omega_{Tm}=\omega_0$, $\omega_a=1.09\omega_0$, and $\gamma_e=\gamma_m=10^{-10}\omega_0$. Here, ω_0 is a scaling parameter. Then, $\mu_3(\omega_a)=\varepsilon_3(\omega_a)\approx-1.99+1.73\times10^{-9}i$.

$$\Gamma_{gz}^p=\frac{3\pi\gamma_0}{4|\varepsilon_3|}\sum_m \left.\frac{k^2\{1+\cos[2(\beta_3 z_0'+\phi_{32}^p)]\}}{\left|d_3'+\frac{\varepsilon_1\varepsilon_3}{\beta_1}\chi_1+\frac{\varepsilon_2\varepsilon_3}{\beta_2}\chi_2\right|}\right|_{k=k_{gp}^{(m)}}, \tag{11}$$

in which $z_0'=z_0\omega/c$, $d_3'=d_3\omega/c$, and γ_0 represents the SE rate of the atom in free space. Further,

$$r_{32}^p=\exp(-2i\phi_{32}^p), \tag{12}$$

with $0\leq\phi_{32}^p\leq\pi/2$, and

$$\chi_i=\frac{\varepsilon_3\mu_3-\varepsilon_i\mu_i}{\varepsilon_i^2\beta_3^2+\varepsilon_3^2\beta_i^2}. \tag{13}$$

The parameters $k_{gq}^{(m)}(m\in\{1,2,\ldots,m_{\max}^p\})$ represent the wave numbers of the mth p-polarized guided modes in the x-y plane, which are the real roots of equation $D_{p3}=0$ within the region of $\sqrt{\eta_1}<k<\sqrt{\eta_3}$. The number of modes is $m_{\max}^p$, which depends on the thickness of the middle layer, the mode polarization, and the material parameters. Evidently, each guided mode corresponds to a standing wave in this structure and the SE rate depends on the position of the atom. With increasing thickness d_3, the contribution of the guided modes to the SE rate exhibits a sharp cusp at the appearance of an extra mode. For the symmetric case $\varepsilon_1=\varepsilon_2$, $\mu_1=\mu_2$, and $z_0=d_3/2$, there is no contribution to the decay rate from the p-polarized modes whose nodes are exactly coincident with the atomic location such that $\beta_3 d_3+2\phi_{32}^p=(2n+1)\pi(n\in\{0,1,2,\ldots\})$. Only modes with an antinode coinciding with the atomic position contribute to the decay rate since then $\beta_3 d_3+2\phi_{32}^p=2n\pi$.

Full numerical results for the guided modes are shown in Fig. 2(b). Note that guided modes may already occur for very thin, even subwavelength, layers, as the Goos-Hänchen

phase shifts (GHPS) at the interfaces between negative and positive layers enhance the phase change induced by the optical path.[30] The second and the third terms in the denominator of Eq. (11) arising from the GHPS are negative, while the first term due to the optical path is positive. Via this cancelling, in z direction the structure effectively acts as a planar cavity with tiny length and large mode density. In Fig. 2, the decay rate is enhanced by about 4 orders of magnitude compared to the free space decay rate for specific waveguide geometries. This is in sharp contrast to the regular dielectric waveguide with $\varepsilon_3, \mu_3 > 0$, where all three terms in the denominator are positive such that the guided modes have only a small density of modes. Thus in a suitable NRI waveguide, the atom spontaneously emits photons into few guided modes with large amplitudes. For an atom placed close to a nanostructure, spontaneous emission can be greatly enhanced due to couplings to electronic quasiparticle surface excitations.[34] But here, the enhancement of some guided modes arises from a variation of the summation of the optical path and the phase changes at the interfaces between negative- and positive-refraction-index materials. Thus these interfaces lead to the strong enhancement.

B. Surface-guided modes

In regular dielectric waveguides, evanescent modes do not contribute to the SE rate as they cannot propagate out. But if one or two of the layers are made from NRI, surface-guided modes with $k^2 > \eta_3$ can exist, whose wave vectors obey the resonance condition $D_{q3}=0$ in the Green's function Eq. (7). Different from the regular positive-index dielectric waveguide, where the magnitudes of the reflection coefficients r_{32}^q and r_{31}^q are smaller than 1, in the NRI waveguide, the modulus of r_{32}^q and r_{31}^q can be larger than 1. Thus real roots $k_{sq}^{(m)} (m \in \{1,2,\ldots\})$ can be found, corresponding to the wave vectors of the surface-guided modes. The contribution of these guided modes to the z component of the dipole moment is

$$\Gamma_{sz}^p = \frac{3\pi\gamma_0}{4|\varepsilon_3|} \sum_m \left. \frac{k^2\{\cosh[2(\beta_3 z_0' - \phi_{32}^{sp})] - 1\}}{\left| d_3' - \frac{\varepsilon_1\varepsilon_3}{\beta_1}\chi_1 - \frac{\varepsilon_2\varepsilon_3}{\beta_2}\chi_2 \right|} \right|_{k=k_{sp}^{(m)}}. \tag{14}$$

Here we have set $r_{32}^p = -\exp(2\phi_{32}^{sp})$ with $\phi_{32}^{sp} \geq 0$. In Eq. (14), the mode functions are hyperbolic instead of the standing-wave functions for the regular-guided modes [Eq. (11)].

By numerical and analytical inspection, we find that there are two kinds of surface-guided modes. The first has a wave vector k^2 close to η_3 while the other one has $k^2 \gg \eta_3$. It can be proven that the surface-guided modes with $k^2 \gg \eta_3$ can only exist when the thickness d_3 of the middle layer is very thin. As an example, we estimate the condition for this kind of surface-guided modes for the symmetric NRI waveguide ($\varepsilon_1 = \varepsilon_2, \mu_1 = \mu_2$). For the p-polarized surface-guided modes, the condition can be approximated as

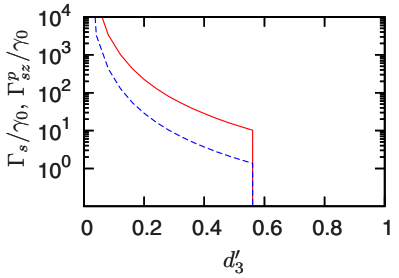

FIG. 3. (Color online) Decay rates into surface-guided modes with total decay-rate contribution Γ_s (solid red line) and contribution Γ_{sz}^p of the p mode (dashed blue line) for z polarization. The parameters are as in Fig. 2.

$$k_{sp}^{(m)} d_3' = \ln \left| \frac{\varepsilon_1 - \varepsilon_3}{\varepsilon_1 + \varepsilon_3} \right|. \tag{15}$$

Therefore p-polarized surface modes with $k^2 \gg \varepsilon_3\mu_3$ may exist only if the thickness d_3 obeys $d_3' \ll \ln|(\varepsilon_1 - \varepsilon_3)/(\varepsilon_1 + \varepsilon_3)|/\eta_3$, i.e., d_3 is much smaller than one wavelength. For these surface modes, Eq. (14) reduces to

$$\Gamma_{sz}^p = \frac{3\pi\gamma_0}{4|\varepsilon_3|} \sum_m \left. \frac{k^2\{\cosh[\beta_3(d_3' - 2z_0')] - 1\}}{\left| d_3' - \frac{2\varepsilon_1\varepsilon_3(\varepsilon_3\mu_3 - \varepsilon_1\mu_1)}{k^3(\varepsilon_1^2 - \varepsilon_3^2)} \right|} \right|_{k=k_{sp}^{(m)}}. \tag{16}$$

We can see that if $z_0' \neq d_3'/2$ then the decay rate can be large, as shown in Fig. 3, as this mode only survives for thin d_3 with a large amplitude. This large enhancement of surface-guided mode excitation enables dipole emission to be preferentially coupled to the surface-guided modes, which may be applied in creating well-guided light sources at the nanoscale.

Regarding the second type of surface-guided modes with k^2 close to η_3, it can be found that these modes may exist if

$$d_3' \leq d_3^{\max} = -\frac{2\varepsilon_1}{\varepsilon_3\sqrt{\varepsilon_3\mu_3 - \varepsilon_1\mu_1}}. \tag{17}$$

This is the reason for the sharp cutoff visible for the solid curves in Fig. 3. The decay rate induced by these p-polarized surface-guided modes can be approximated as

$$\Gamma_{sz}^p = \frac{3\pi\gamma_0|\mu_3|}{8} \sum_m \frac{[(k_{sp}^{(m)})^2 - \varepsilon_3\mu_3](d_3' - 2z_0')^2}{|d_3' - d_3^{\max}|}. \tag{18}$$

In thin waveguides, these contributions are small as compared to those of Eq. (16), due to the difference of the mode amplitudes.

Thus for thin NRI waveguides, the atom can emit strong evanescent fields with large wave number $k^2 \gg \eta_3\mu_3$ in the x-y plane. This result is similar to experimental evidence employing a pristine silver film with natural roughness as a NRI slab,[35] where the transmission of evanescent waves rapidly grows with the NRI film thickness up to a thickness of about $\lambda/10$.

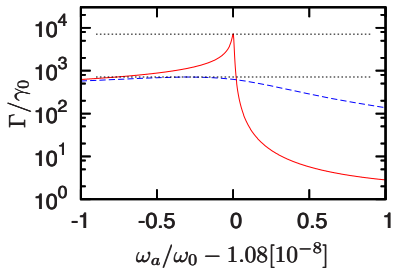

FIG. 4. (Color online) The influence of dispersion and absorption on the results. The red solid line shows the frequency dependence of the total decay rate for parameters as in Fig. 2 but with d_3 set to the first peak in Γ_z^p. The blue dashed line is plotted for same parameters but includes small absorption $\gamma=\gamma_e=\gamma_m=10^{-8}\omega_0$. The black horizontal dotted lines indicate the peak amplitudes of about $7100\gamma_0$ and $710\gamma_0$, respectively, of the two curves, verifying the scaling of the peak amplitudes with $1/\sqrt{\gamma}$.

C. Dispersion and absorption

With absorption and dispersion, the above equations are more complex. Then, the sharp peaks due to the guided modes become Lorentzians, with widths depending on the imaginary part of the refraction index. For small $\gamma=\gamma_e=\gamma_m$, their amplitudes are proportional to $1/\sqrt{\gamma}$. This scaling generalizes our results to moderate absorption strengths. An example is shown in Fig. 4. This figure shows a magnification on the first peak at $d_3'\approx 3$ in the waveguide decay Γ_{gz}^p shown in Fig. 2. It can be seen that with increasing absorption, the narrow peak is broadened such that the peak amplitude is reduced, in accordance with our scaling law. In contrast to Fig. 2, in Fig. 4 the frequency dependence of the results is shown in order to analyze the dispersive properties of the NRI waveguide.

We now turn to the case of high absorption. An example for decay into radiation modes in a strongly absorbing waveguide is shown in Fig. 5(a). The corresponding results for waveguide modes and special guided modes are shown in Figs. 5(b) and 6. It can be seen that while the waveguide modes are strongly reduced to peak decay rates of order γ_0, the radiation modes and special guided modes are much less affected by the absorption. Speaking pictorially, the absorption leads to a washing out of narrow structures found in the waveguide modes, such that their amplitude is strongly reduced with increasing absorption. In contrast, the structures in the radiation and special guided modes are already rather broad at low absorption such that they do not change much toward higher absorption.

D. Quantum interference

Finally, we evaluate the cross-coupling terms κ_n in Eq. (4), which are responsible for SE interference. The strong enhancement of decay into particular guided modes at low absorption can be used to generate controllable near-perfect quantum interference, i.e., $\kappa\approx\pm 1$, as shown in Fig. 7(a). If both transitions mainly interact with the same strongly enhanced guided mode, then they couple even though they have orthogonal transition dipole moments. For example, if d_3' is chosen close to the birth of a s-polarized mode but

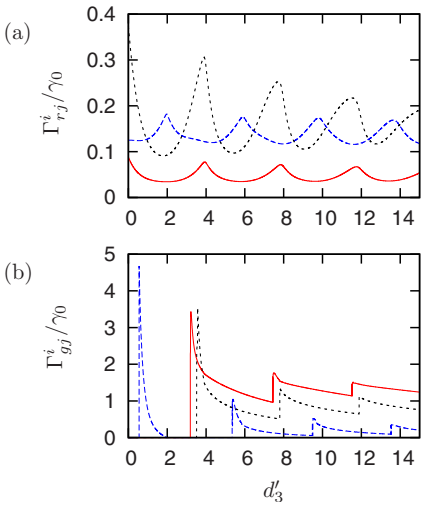

FIG. 5. (Color online) Spontaneous emission into strongly absorbing NRI waveguides. (a) Radiation mode contributions Γ_{rz}^p (solid red line), Γ_{rx}^p (dashed blue line) and Γ_{rx}^s (dotted black line). (b) Waveguide mode contributions Γ_{gz}^p (solid red line), Γ_{gx}^p (dashed blue line) and Γ_{gx}^s (dotted black line). The atom is located at $z_0'=0.5d_3'$ and the material parameters are $\varepsilon_1=\varepsilon_2=\mu_1=\mu_2=1.0$, $\omega_{pe}=1.25\omega_0$, $\omega_{pm}=1.189\omega_0$, $\omega_{Te}=\omega_{Tm}=\omega_0$, $\omega_a=1.08\omega_0$, and $\gamma_e=\gamma_m=10^{-3}\omega_0$. Here, ω_0 is a scaling parameter. Then, $\varepsilon_3(\omega_a)\approx -2.38+2.19\times 10^{-2}i$ and $\mu_3(\omega_a)\approx -1.48+1.61\times 10^{-2}i$.

away from p-polarized mode maxima then the decay rate is dominated by Γ_x^s induced by the s-polarized modes to the x component of the atomic dipole. It follows from Eq. (6) that then $\kappa\approx -1$, i.e., strong quantum interference similar to that of a hypothetical atom having two near-degenerate transitions with near-antiparallel dipole matrix elements in free space.[1,3–7] A second example is for atoms located at the center of the NRI layer with d_3' set at the birth of a p-polarized mode. If $\beta_3 d_3'+2\phi_j^p=(2n+1)\pi$, then the decay rate is dominated by Γ_{gx}^p from the x component of the atomic dipole as the atom is at the node of the z modes. But for $\beta_3 d_3'+2\phi_j^p=2n\pi$, it is dominated by Γ_{gz}^p as the atom is at the node of the x modes. These situations yield strong quantum interference with $\kappa\approx\pm 1$, similar to near-(anti)parallel dipole moments in free space. Both cases are shown in Fig. 7(a). The extremal values of κ occur at peaks in the SE rate due to the enhanced mode density and thus d_3' controls κ between -1 and 1. In Fig. 7(a), we have used $\varepsilon_3\neq\mu_3$ to enable the first mechanisms for extremal κ and $z_0'=d_3'/2$ to allow for the

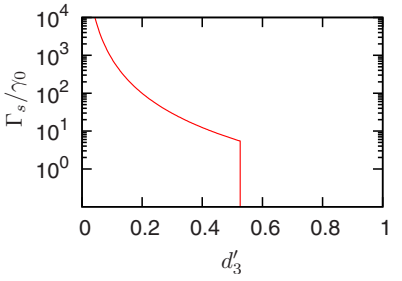

FIG. 6. (Color online) Decay rates into surface-guided modes. The total decay rate Γ_s has contribution only from Γ_{sx}^p of the p mode for x polarization. The parameters are as in Fig. 5.

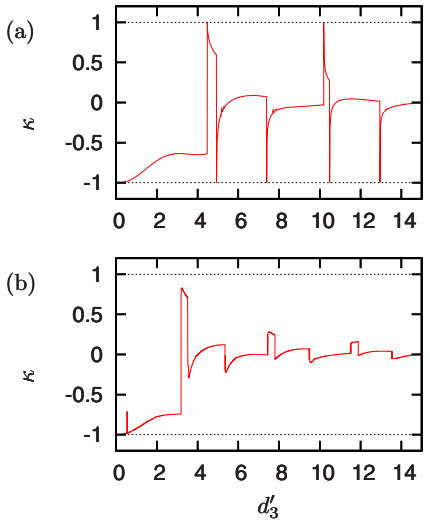

FIG. 7. (Color online) Quantum interference induced by a negative-refraction-index waveguide structure characterized by the interference strength κ. (a) Parameters as in Fig. 2 except for $z_0'=d_3'/2$, $\omega_{pm}=1.189\omega_0[\mu_3(\omega_a)\approx-1.20+1.27\times10^{-9}i]$. (b) Strong absorption case. Parameters are as in Fig. 5 with $\varepsilon_3(\omega_a)\approx-2.38+2.19\times10^{-2}i$ and $\mu_3(\omega_a)\approx-1.48+1.61\times10^{-2}i$.

second mechanism. Thus NRI waveguide structures allow us to effectively induce spontaneous emission quantum interference with realistic atomic-level structures.

Interestingly, spontaneous emission interference can already be obtained at high absorption even though in this case the narrow peaks of large amplitude are absent from the waveguide mode spectrum. An example is shown in Fig. 7(b) for the parameters of Fig. 5. In particular, at small thicknesses d_3' of the waveguide, a large degree of interference is achieved ($\kappa\approx-1$). The reason for this is the dominant contribution of the special guided modes. For the particular setup chosen in this figure, only special waveguides in the p-x mode are excited. But also at larger thicknesses, interference of alternating sign in κ is achieved even though with $|\kappa|$ smaller than unity. This has to be compared, however, to a value of $\kappa=0$ for atoms in free space.

IV. DISCUSSION AND SUMMARY

Our results indicate that a negative-index waveguide could be an attractive implementation of spontaneously generated coherences in atomic or molecular systems. This is particularly interesting in view of the many applications that have been suggested theoretically in the literature[1,2] and of the lack of other experimental implementations. The embedding of the quantum particle in a host layer at the same time would provide convenient trapping even for neutral particles. Depending on the structure of the waveguide, very different decay characteristics can be tailored for the same atom or molecule, which adds an interesting degree of freedom to the application of coherence and interference effects in quantum optics.

At present, implementation of negative-index materials usually involves so-called metamaterials, which are artificial materials designed to exhibit the desired optical response. Due to their artificial nature, the unit-cell size of metamaterials can be significantly larger than that of natural materials. On the other hand, as in most previous related treatments, our analysis is based on the assumption that the considered materials are homogeneous. This allows us to describe the materials via dielectric functions [Eq. (3)]. The requirement of homogeneity essentially translates to a restriction of the involved length scales. In particular, the size of the unit cells of the artificial metamaterial has to be small as compared to the atom-surface distance and the relevant emission wavelengths.[25] This remains challenging in the optical and near-optical region despite the tremendous progress in fabricating nanosized metamaterials. In a recent experiment, a refractive index of $\mathrm{Re}(n)=-1$ was achieved at a wavelength of about 1.7 μm in a bulk metamaterial with unit-cell size below 1 μm.[36] Other available implementations operating at longer wavelengths are more promising. For example, a bulk material was reported with negative-refractive index $\mathrm{Re}(n)=-1.6$ and linear unit-cell dimension $a=60$ μm.[37] The resonance frequency is 1.03 THz, corresponding to a wavelength of about $\lambda=300$ μm. This transition frequency, e.g., is in the range of the first rotational transition of a NH molecule.[25] Also other aspects of metamaterials have been considered in the literature. For example, the specific composition of the material can lead to a modified dielectric function and metamaterials in general are anisotropic.[38]

In conclusion, we have investigated the spontaneous decay of a three-level V-type atom placed in a three-layer waveguide with negative-refraction-index material as middle layer. We have found that spontaneous emission into particular guided modes can be greatly enhanced in materials with low losses. Due to a large mode density, spontaneous decay rates into these modes can be increased by several orders of magnitude as compared to regular dielectric waveguides. Both at low and high absorptions, NRI waveguides support additional surface-guided modes, which do not occur in positive index waveguides. The modes also offer a strong enhancement of spontaneous decay compared to the free space case and are especially effective in thin waveguides. The specific properties of the waveguide as well as the position of the atom in the waveguide enable one to modify the emission into the different modes to a great extend. We have shown that this control can be used to achieve asymmetries in the decay into modes with different polarizations. This feature allows us to induce strong spontaneous emission interference in realistic atomic-level schemes, which do not exhibit such interference in free space.

In addition to NRI waveguides, we also analyzed airlike waveguides with NRI cladding.[26] In these structures, the middle layer is airlike while the upper and the lower layer are made of NRI material. We obtained similar results as for the NRI waveguides. In particular, also in this case the density of the guided modes and thus SE can be very large if the absorption is low.

ACKNOWLEDGMENTS

G.-x.L. gratefully acknowledges financial support from

the Alexander von Humboldt Foundation, the National Natural Science Foundation of China under Grants No. 10674052 and No. 80878004, and the Ministry of Education under project NCET under Grant No. NCET-06-0671. J.E. gratefully acknowledges hospitality during his stay in Huazhong Normal University. Helpful discussions with S. Y. Zhu are gratefully acknowledged.

*gaox@phy.ccnu.edu.cn
†joerg.evers@mpi-hd.mpg.de

[1] Z. Ficek and S. Swain, *Quantum Interference and Coherence* (Springer, Berlin, 2005).
[2] M. O. Scully and M. S. Zubairy, *Quantum Optics* (Cambridge University Press, Cambridge, 1997).
[3] S. Y. Zhu and M. O. Scully, Phys. Rev. Lett. **76**, 388 (1996).
[4] P. Zhou and S. Swain, Phys. Rev. Lett. **77**, 3995 (1996); C. H. Keitel, *ibid.* **83**, 1307 (1999).
[5] E. Paspalakis, N. J. Kylstra, and P. L. Knight, Phys. Rev. Lett. **82**, 2079 (1999).
[6] M. Macovei, J. Evers, and C. H. Keitel, Phys. Rev. Lett. **91**, 233601 (2003).
[7] O. Kocharovskaya, A. B. Matsko, and Y. Rostovtsev, Phys. Rev. A **65**, 013803 (2001).
[8] G. S. Agarwal, Phys. Rev. Lett. **84**, 5500 (2000); J. Evers and C. H. Keitel, *ibid.* **89**, 163601 (2002); **92**, 159303 (2004); P. R. Berman, *ibid.* **92**, 159301 (2004); A. G. Kofman, *ibid.* **92**, 159302 (2004); J. Evers and C. H. Keitel, J. Phys. B **37**, 2771 (2004).
[9] H.-R. Xia, C.-Y. Ye, and S.-Y. Zhu, Phys. Rev. Lett. **77**, 1032 (1996).
[10] L. Li, X. Wang, J. Yang, G. Lazarov, J. Qi, and A. M. Lyyra, Phys. Rev. Lett. **84**, 4016 (2000).
[11] M. V. G. Dutt, Jun Cheng, Bo Li, Xiaodong Xu, Xiaoqin Li, P. R. Berman, D. G. Steel, A. S. Bracker, D. Gammon, Sophia E. Economou, Ren-Bao Liu, and L. J. Sham, Phys. Rev. Lett. **94**, 227403 (2005).
[12] M. Kiffner, J. Evers, and C. H. Keitel, Phys. Rev. Lett. **96**, 100403 (2006); Phys. Rev. A **73**, 063814 (2006).
[13] A. M. Akulshin, S. Barreiro, and A. Lezama, Phys. Rev. A **57**, 2996 (1998); A. V. Taichenachev, A. M. Tumaikin, and V. I. Yudin, *ibid.* **61**, 011802 (1999); L. Spani Molella, R.-H. Rinkleff, and K. Danzmann, *ibid.* **72**, 041802(R) (2005).
[14] E. M. Purcell, Phys. Rev. **69**, 681 (1946); S. Haroche and D. Kleppner, Phys. Today **42**(1), 24 (1989).
[15] S. A. Ramakrishna, Rep. Prog. Phys. **68**, 449 (2005).
[16] J. B. Pendry, Phys. Rev. Lett. **85**, 3966 (2000); E. Cubukcu, Koray Aydin, Ekmel Ozbay, Stavroula Foteinopoulou, and Costas M. Soukoulis, Nature (London) **423**, 604 (2003); A. Grbic and G. V. Eleftheriades, Phys. Rev. Lett. **92**, 117403 (2004).
[17] D. R. Smith, W. J. Padilla, D. C. Vier, S. C. Nemat-Nasser, and S. Schultz, Phys. Rev. Lett. **84**, 4184 (2000); S. Zhang, W. Fan, B. K. Minhas, A. Frauenglass, K. J. Malloy, and S. R. J. Brueck, *ibid.* **94**, 037402 (2005); S. Zhang, W. Fan, N. C. Panoiu, K. J. Malloy, R. M. Osgood, and S. R. J. Brueck, *ibid.* **95**, 137404 (2005).
[18] Y. F. Chen, P. Fischer, and F. W. Wise, Phys. Rev. Lett. **95**, 067402 (2005).
[19] M. Bloemer, G. D'Aguanno, M. Scalora, and N. Mattiucci, Appl. Phys. Lett. **87**, 261921 (2005).
[20] H. Li, J. Hao, L. Zhou, Z. Wei, L. Gong, H. Chen, and C. T. Chan, Appl. Phys. Lett. **89**, 104101 (2006).
[21] J. Kästel and M. Fleischhauer, Phys. Rev. A **71**, 011804(R) (2005).
[22] Y. P. Yang, J. P. Xu, H. Chen, and S. Y. Zhu, Phys. Rev. Lett. **100**, 043601 (2008).
[23] B. I. Wu, T. M. Grzegorczyk, Y. Zhang, and J. A. Kong, J. Appl. Phys. **93**, 9386 (2003); I. V. Shadrivov, A. A. Sukhorukov, and Y. S. Kivshar, Phys. Rev. E **67**, 057602 (2003); J. Schelleng, C. Monzon, P. F. Loschialpo, D. W. Forester, and L. N. Medgyesi-Mitschang, *ibid.* **70**, 066606 (2004).
[24] J.-P. Xu, Y.-P. Yang, Q. Lin, and S. Y. Zhu, Phys. Rev. A **79**, 043812 (2009).
[25] A. Sambale, D.-G. Welsch, H. T. Dung, and S. Y. Buhmann, Phys. Rev. A **78**, 053828 (2008).
[26] G. D'Aguanno, N. Mattiucci, M. Scalora, and M. J. Bloemer, Phys. Rev. E **71**, 046603 (2005).
[27] B. Prade, J. Y. Vinet, and A. Mysyrowicz, Phys. Rev. B **44**, 13556 (1991).
[28] J. L. van Velsen, J. Tworzydlo, and C. W. J. Beenakker, Phys. Rev. A **68**, 043807 (2003); S. Fasel, F. Robin, E. Moreno, D. Erni, N. Gisin, and H. Zbinden, Phys. Rev. Lett. **94**, 110501 (2005); A. V. Akimov, A. Mukherjee, C. L. Yu, D. E. Chang, A. S. Zibrov, P. R. Hemmer, H. Park, and M. D. Lukin, Nature (London) **450**, 402 (2007); D. E. Chang, A. S. Sorensen, E. A. Demler, and M. D. Lukin, Nat. Phys. **3**, 807 (2007); M. S. Tame, C. Lee, J. Lee, D. Ballester, M. Paternostro, A. V. Zayats, and M. S. Kim, Phys. Rev. Lett. **101**, 190504 (2008).
[29] D. E. Chang, A. S. Sorensen, P. R. Hemmer, and M. D. Lukin, Phys. Rev. Lett. **97**, 053002 (2006).
[30] I. V. Shadrivov, A. A. Zharov, and Y. S. Kivshar, Appl. Phys. Lett. **83**, 2713 (2003); D. K. Qing and G. Chen, Opt. Lett. **29**, 872 (2004).
[31] H. T. Dung, S. Y. Buhmann, L. Knöll, D.-G. Welsch, S. Scheel, and J. Kästel, Phys. Rev. A **68**, 043816 (2003).
[32] M. S. Tomas, Phys. Rev. A **51**, 2545 (1995); G. X. Li, F. L. Li, and S. Y. Zhu, *ibid.* **64**, 013819 (2001); L. Zhou and G. X. Li, Opt. Commun. **230**, 347 (2004).
[33] J. Pacheco, T. M. Grzegorczyk, B.-I. Wu, Y. Zhang, and J. A. Kong, Phys. Rev. Lett. **89**, 257401 (2002).
[34] I. V. Bondarev, G. Ya. Slepyan, and S. A. Maksimenko, Phys. Rev. Lett. **89**, 115504 (2002); L. A. Blanco and F. J. Garcia de Abajo, Phys. Rev. B **69**, 205414 (2004).
[35] Z. Liu, N. Fang, T. J. Yen, and X. Zhang, Appl. Phys. Lett. **83**, 5184 (2003).
[36] J. Valentine, S. Zhang, T. Zentgraf, E. Ulin-Avila, D. A. Genov, G. Bartal, and X. Zhang, Nature (London) **455**, 376 (2008).
[37] O. Paul, C. Imhof, B. Reinhard, R. Zengerle, and R. Beigang, Opt. Express **16**, 6736 (2008).
[38] F. S. S. Rosa, D. A. R. Dalvit, and P. W. Milonni, Phys. Rev. Lett. **100**, 183602 (2008).